15TH IEA HEAT PUMP CONFERENCE
MAY 26–29, 2026 | HOFBURG
VIENNA 2026
DECARBONISATION THROUGH INNOVATION

"Numerical Investigation and Design of a Test Stand for a High Temperature Heat Pump up to 200 °C"

Andrew LeBlanc[1], Darshak Gadagkar[1], Andreas J. Hoess[1], Davide Ziviani[1], Riley B. Barta[1]

[1]Ray W. Herrick Laboratories, School of Mechanical Engineering, Purdue University, West Lafayette, IN, 47907, USA

Abstract

High-temperature heat pumps (HTHPs) are essential for improving the efficiency of industrial heating processes. Increasing the HTHP supply temperatures can enable a broader impact of the technology on different industrial sectors, but also has challenges associated with cycle efficiency, compression technologies, and material compatibilities. This study presents the modeling efforts to design and develop a state-of-the-art test facility with a novel HTHP architecture with the goal of producing heat at 200 °C with a subcritical cycle. Specifically, the cycle features refrigerant economization coupled with internally cooled rotors in an additively manufactured twin-screw compressor for enhanced discharge temperature control and efficiency. Potential refrigerant candidates were filtered based on a previous refrigerant screening and the refrigerant that yielded the best results was pure cyclopentane. Increased model fidelity was achieved by integrating a compressor map and segmented heat exchanger models, resulting in a predicted system COP of 2.85, Second Law efficiency of 48.7%, and an outlet heat sink temperature of 201 °C. The numerical investigations have been employed to design the test stand that will be used to validate the cycle's performance and to demonstrate safe operation with cyclopentane. The test setup will confirm the ability to reach 200 °C heat sink temperatures, assess refrigerant and lubricant compatibility, and explore compressor behavior and material compatibility at high temperatures. This integrated work demonstrates the feasibility of this cycle architecture and supports its role in maximizing HTHP efficiency for industrial applications.

Keywords: High-temperature heat pump; low-GWP; waste heat recovery; vapor compression cycle

1. Introduction

Industrial processes are energy-intensive and accounted for approximately 35% of total U.S. primary energy consumption in 2022 [1]. Process heat is responsible for a considerable share of that consumption, which totalled 73% of industrial energy demand in the EU in 2012 [2]. Currently, this worldwide industrial heat demand is mostly met with coal and natural gas–fired boilers, making the sector a major contributor to global emissions. Roughly 47% of total CO_2 emissions were the result of heat and electricity consumed by industrial activity in 2023 [3].

High-temperature heat pumps (HTHPs) offer a means for improving process efficiencies by upgrading low-temperature waste heat produced in industrial settings to the higher temperatures required by various industrial processes. HTHPs are particularly well suited for applications in the food and beverage, paper and pulp, chemical, and refinery sectors. An estimate of waste and process heat distribution below 200 °C for the EU28 is presented in Figure 1. Total available waste heat was calculated to be 1,130 PJ/a, and the total process heat demand was calculated to be 1,123 PJ/a. According to the authors, industrial heat pumps could supply 641 PJ/a, more than half of this demand [4]. The remaining, uncovered demand primarily comprises processes where temperature lift exceeds 100 °C, which the authors considered prohibitively high with current technologies.

Globally, Technavio (2024) has predicted HTHPs to grow at a 5.8% on average between 2024 and 2029 [5]. The American Council for an Energy Efficient Economy found that HTHPs can reduce the energy consumption associated with process heat by up to 33%, preventing 30-43 million tons of CO_2 from being

15th IEA Heat Pump Conference 2026 - HTH3.3 - https://doi.org/10.23697/r7wm-re19

emitted each year [6]. A summary of existing prototypes and commercially available HTHPs is shown in Figure 2.

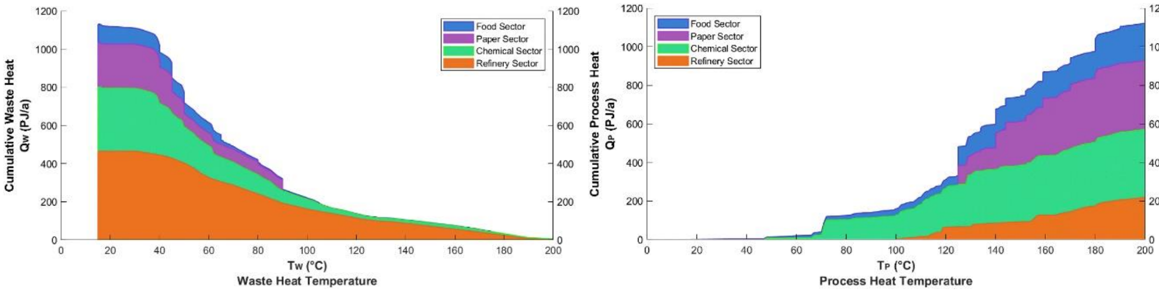

Figure 1. Cumulative waste and process heat below 200 °C in the EU28 identified in the most relevant industries for HTHPs [4].

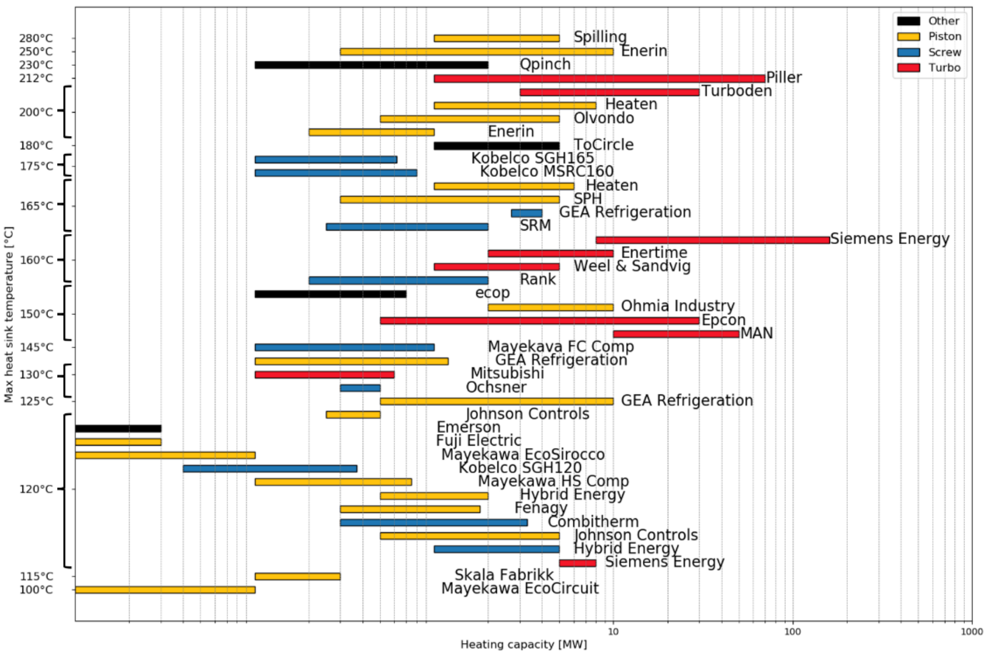

Figure 2. Commercially available HTHPs displayed by maximum heat sink temperature and heating capacity. Adapted from Arpagaus, 2023 [7].

While heat pump manufacturers have been able to achieve heat sink temperatures exceeding 200 °C, this has primarily been done utilizing piston and turbo compressors. A gap remains in achieving 200 °C supply temperatures via the use of a screw compressor. The primary purpose of this study is to develop a HTHP that can bridge that gap.

There is limited literature regarding the modelling of HTHPs, particularly at temperatures approaching 200 °C. Kondou and Koyama (2015) compared four different cycles using four different hydrofluoroolefin (HFO) refrigerants to upgrade heat provided by a pressurized water source at 80 °C to 160 °C. Simplified pinch point models were used for the heat exchangers and compressor efficiencies were assumed to be independent of pressure ratio and rotational speed. The study found a multi-stage extraction cycle utilizing R-1234ze(Z) to have the highest coefficient of performance (COP) out of the combinations investigated [8].

Kosmadakis et al. (2020) analysed single and two-stage cycles employing low global warming potential (GWP) refrigerants for use in HTHPs upgrading waste heat from below 100 °C to 150 °C. Their model employed moving boundary models and experimentally derived correlations for isentropic and volumetric efficiencies for a semi-hermetic screw compressor. R-1234ze(Z) delivered the highest heating capacity but was limited by discharge temperatures due to its relatively low critical temperature of 150.1 °C. R-1336mzz(Z) performed worse in terms of capacity but was identified to be better suited for high temperature applications [9].

Arpagaus et al. (2020) investigated internal heat exchanger (IHX)- and parallel compression-based transcritical cycles for process heat delivery up to 200 °C. HFO refrigerants as well as the hydrocarbons R-600 and R-601 were investigated. The model used discretised heat exchanger models and a fixed compressor isentropic efficiency. The study identified R-1233zd(E), R-1224yd(Z) and R-600 as viable options due to their high volumetric heating capacities and relatively low pressure ratios [10].

Each of these studies illustrates the significant amount of work being done in modelling HTHPs for industrial applications. Nonetheless, important gaps remain. While transcritical cycles up to 200 °C have been modelled, for example, such a study for subcritical cycles has yet to be performed. Additionally, moving boundary models and compressor maps have been employed for HTHPs up to 150 °C, but not yet to 200 °C. Extending the temperature range to 200 °C in a high-fidelity cycle model enables analysis of a larger subset of industrial applications and aids in characterization from the component to system level.

This study aims to develop a test stand implementing a novel cycle architecture called the HERRICK cycle, which features internal cooling of screw compressor rotors using refrigerant flow, among other performance enhancing measures. A high-fidelity cycle model employing moving boundary heat exchanger models and a compressor map was developed. The numerical results of this study inform the test stand component selection and design. The test stand will confirm the feasibility of reaching 200 °C and provide insights into material performance and lubricant compatibility at high temperatures. The presented analysis is based on work performed by Gadagkar (2025) [11].

2. Methodology

2.1. Refrigerant selection

The low-GWP refrigerant screening work conducted by Spale et al. (2024) serves as the basis for this project. Their study evaluated over 460,000 refrigerant mixtures, ranging from binary to quaternary combinations, to identify the most promising candidate for use in a sub-critical vapor-compression HTHP designed for process heat delivery at 200 °C. The screening used an advanced cycle architecture featuring an IHX and an economizer. A steady-state model based on heat and mass balances was implemented in Python using the REFPROP v10 library [12].

The study concluded that a binary mixture of cyclopentane and R-1336mzz(Z), with molar fractions of 0.68 and 0.32, respectively, was the most favorable blend for the given boundary conditions. Because the chosen cycle architecture closely resembles the HERRICK cycle, this mixture was initially selected as the working fluid for HERRICK. However, property testing at NIST revealed that the two fluids could separate under certain conditions. Pure cyclopentane was ultimately selected for use in the test stand as it constitutes the primary component of the optimal but physically unfeasible blend of cyclopentane and R-1336mzz(Z).

2.2. Cycle description

The HERRICK cycle is a novel cycle architecture employing two-stage compression with a suction line heat exchanger (SLHX), economizer and, most notably, internal refrigerant cooling of the compressor rotors. A schematic of the cycle is shown in Figure 3**.**

The SLHX provides internal heat recovery between the high-pressure liquid refrigerant used to cool the compressor rotors and the low-pressure vapor entering the compressor. This recovery increases the superheating of the suction vapor, preventing wet compression that can occur with certain hydrocarbons, and increases the subcooling of the liquid entering the expansion valve, improving the system COP via an increased specific enthalpy change across the evaporation process and thus, an increased cooling capacity for a given compressor mass flow rate.

The economizer exchanges heat between the high-pressure liquid stream exiting the condenser and a secondary intermediate pressure two-phase stream. The secondary stream consists of a small fraction of the liquid exiting the condenser that is expanded to an intermediate pressure. Economization serves to sub-cool the high-pressure liquid stream and superheat the intermediate pressure vapor stream. The intermediate pressure vapor stream is injected during the compression process, allowing control over the internal states of the compressor. This injection reduces compressor discharge temperature and work but must be balanced so as to not inadvertently lead to wet compression at the mixing port or discharge.

The most novel aspect of the HERRICK cycle is the internal cooling of the compressor rotors. This cooling is achieved via the diversion of a small portion of the subcooled high-pressure liquid stream exiting the economizer. The diverted stream passes through internal channels in the screw rotors, providing notable cooling and reducing discharge temperature in an effort to approach isothermal compression.

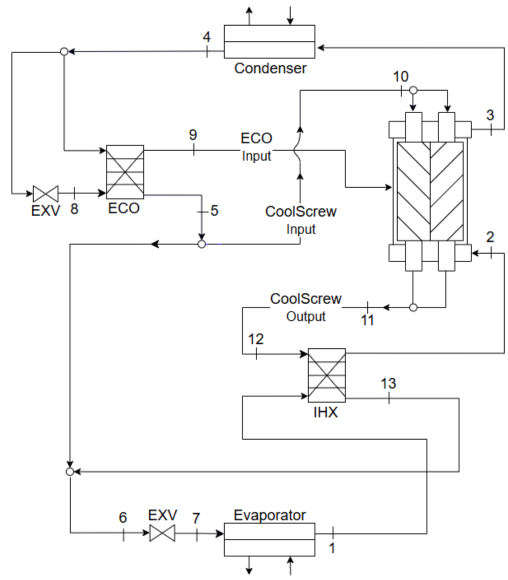

Figure 3. Schematic of the HERRICK cycle.

Test stand boundary conditions

The boundary conditions for the test stand are shown in Table 1. The heat source and sink parameters were determined by the physical limitations of the facility where the test stand is to be built. The condenser bubble point temperature and evaporator dew point temperature were dictated by the design goals of the system.

Table 1. Boundary conditions for the HERRICK cycle test stand.

Parameter	Value	Unit
Condenser bubble point temperature	200	°C
Evaporator dew point temperature	110	°C
Heat source inlet temperature	120	°C
Heat sink inlet temperature	174	°C
Condenser outlet subcooling	5	K
Evaporator outlet superheating	5	K
Condenser minimum approach temperature difference	3	K
Evaporator minimum approach temperature difference	3	K
Economizer minimum approach temperature difference	3	K
SLHX minimum approach temperature difference	3	K
Internal refrigerant rotor cooling	3	kJ/kg

2.3. Compressor modeling

Ma et al. (2011) demonstrated that polynomial correlations can accurately predict compressor isentropic and volumetric efficiencies as a function of pressure ratio PR [13]. The pressure ratio is calculated as the ratio between the condensing pressure P_{cond} and evaporating pressure P_{evap} of the system as shown in Eq. (1).

$$PR = \frac{P_{cond}}{P_{evap}} \tag{1}$$

These efficiency maps are generated by fitting polynomial models to manufacturer-provided performance data reporting efficiencies at various pressure ratios and compressor speeds. For this study, the Thermo King QS319T compressor, with available data for R-407C and R-134a, served as the baseline for developing efficiency correlations. Because no such data is available for cyclopentane, a 10% reduction was applied to both isentropic and volumetric efficiencies to approximate compressor performance. The correlations for isentropic and volumetric compressor efficiency at 2,000 RPM are shown in Eq. (2) and Eq. (3), respectively.

$$\eta_{is} = -0.775 + 1.083(PR) - 0.325(PR^2) + 0.052(PR^3) - 0.004(PR^4) + 10^{-4}(PR^5) \tag{2}$$

$$\eta_{vol} = 0.9020 + 0.0078(PR) - 0.0008(PR^2) + 0.0001(PR^3) \tag{3}$$

Having defined isentropic and volumetric efficiency correlations, the thermodynamic properties of each compression state can be determined. Since these correlations are based on manufacturer test data obtained under non-adiabatic conditions, the efficiencies do not represent purely adiabatic performance. Accordingly, an additional 10% penalty represented by a factor f is imposed to approximate heat losses. The specific enthalpy at the outlet of the first compression stage h_3 is determined via the isentropic efficiency η_{is} given by the compressor correlations at the corresponding pressure ratio. This relation is shown in Eq. (4). h_2 represents the specific enthalpy at the compressor inlet and h_{3s} represents the specific enthalpy at the first discharge state assuming an isentropic compression process.

$$h_3 = h_2 + \frac{(1-f)(h_{3s}-h_2)}{\eta_{is}} \tag{4}$$

With the condensing and evaporating boundary conditions specified, and the isentropic and volumetric efficiency maps defined, the required mass flow rate $\dot{m}$ can be calculated as shown in Eq. (5). $\dot{V}$ represents the volumetric flow rate and $\rho_{suction}$ represents the density of the fluid at the compressor inlet.

$$\dot{m} = \dot{V}\rho_{suction} \tag{5}$$

2.4. Moving boundary heat exchanger model

The moving boundary model discretizes heat exchangers into segments according to fluid phase. This allows for more accurate characterization than using a lumped approach because phase- and flow-specific correlations can be applied to more accurately characterize pressure drop and heat transfer behaviors associated with a specific flow type. The refrigerant may exist in either single or two-phase regions while undergoing evaporation or condensation. Accurately capturing the relative length of the regions for a given phase of flow is critical in predicting overall heat exchanger effectiveness. To calculate these relative lengths, the detailed cycle model ACHP+ for plate heat exchangers was used with minor modifications [14,15].

The inputs to the model are the inlet states and mass flow rates of each fluid as well as the geometric parameters of the heat exchangers. The first step is to determine the maximum possible heat transfer rate Q_{max} between the two fluids, which is done by assuming 100% effectiveness, where the outlet temperature of each fluid reaches the inlet temperature of the other. Next, violations of the second law, where Q_{max} creates a physically impossible temperature inversion somewhere along the length of the heat exchanger, are checked. If there is such an inversion, Q_{max} is reduced until the temperatures at the pinch point are equal. The updated Q_{max} is used in an iterative one-dimensional solver to determine the actual heat transfer rate that satisfies the energy balance. The solver builds enthalpy vectors for each stream, determining phase transition locations and computing the fraction of heat exchanger length w_i associated with each phase region. Within each region, appropriate correlations are applied to determine local heat transfer coefficient and pressure drop. The relevant correlations for each type of flow are detailed in the following sections.

2.4.1. Single-phase flow

For regions of single-phase flow, the analysis from Martin (2010) is utilized [16]. Correlations for the Nusselt number Nu are provided, allowing the heat transfer coefficient HTC to be calculated via Eq. (6). k represents the thermal conductivity of the fluid and d_h represents the hydraulic diameter.

$$HTC = \frac{kNu}{d_h} \tag{6}$$

Pressure drop is determined via the dimensionless Hagen number Hg. The Hagen number is dependent on the Reynold's number and the friction factor. The Reynold's number Re is calculated via Eq. (7), where ρ, w and μ are the density, velocity, and dynamic viscosity of the fluid, respectively. Martin (2010) gives correlations to be used for friction factor ξ. With these parameters defined, the Hagen number is calculated as shown in Eq. (8), where Δp is the pressure drop and L_p is the length of the plate. Eq. (8) is re-arranged to solve for pressure drop in Eq. (9).

$$Re = \frac{\rho w d_h}{\mu} \tag{7}$$

$$Hg = \frac{\xi Re^2}{2} = \frac{\rho \Delta p d_h^3}{\mu^2 L_p} \tag{8}$$

$$\Delta p = Hg \frac{\mu^2 L_p}{\rho d_h^3} \tag{9}$$

2.4.2. Two-phase evaporating flow

Two-phase evaporating flow is more difficult to model than single-phase flow and requires the use of correlations from the literature. According to Bell (2011), the currently accepted understanding of evaporating flow in plate heat exchangers is that nucleate boiling dominates. Thus, the Cooper (1984) pool boiling correlation is used as shown in Eq. (10) [17]. Scaling factor K is given as 1.5 for brazed plate heat exchangers by Claesson (2004) [18]. The overall heat transfer coefficient *HTC* is dependent upon the reduced pressure $p*$, the surface roughness R_p, the heat flux q'', and the refrigerant molar mass M, shown in Eq. (10).

$$HTC = K55(p^*)^{0.12-0.2\,log_{10} R_p}(-\,log_{10} p^*)^{-0.55}\ (q'')^{0.67}\ M^{-0.5} \tag{10}$$

Frictional pressure drop for two-phase evaporating flow is determined via the Lockhart-Martinelli (1949) correlation [19]. Claesson (2004) suggests a value of 4.67 for the *C* parameter, which is an empirical constant that depends upon the flow regimes of the liquid and gas phases. This parameter is employed along with the Martinelli parameter in calculating the two-phase multipliers necessary to characterize the frictional pressure drop of each phase. Claesson also provides an equation for accelerational pressure drop. Gravitational pressure drop is neglected in this analysis.

2.4.3. Two-phase condensing flow

Two-phase condensing flow in plate heat exchangers suffers from a similar lack of attention in the literature. The plate heat exchanger studies from Longo (2009) provide empirical correlations for the heat transfer coefficient as shown in Eq. (11) [20]. Values for the constant coefficient *j* are provided at different Reynold's numbers and Pr represents the Prandtl number.

$$HTC = \frac{jk\mathrm{Pr}^{1/3}}{d_h}$$

The pressure drop calculations for two-phase condensing flow are the same as those for two-phase evaporating flow.

3. Results

Results regarding compressor and heat exchanger selection for the test stand are detailed in the following sections. Finally, modeling outcomes and the resulting test stand design are discussed.

3.1. Compressor selection

The compressor to be used in the test stand is provided by Trane Technologies, who supplied data for three models: the Thermo King QS391B, QS391T, and QS616B. Mass flow rate, power consumption, discharge temperature, and volumetric and isentropic efficiencies were reported for each model. Data was given for rotational speeds of 1,000, 2,000, and 3,000 RPM. The QS391T was ultimately chosen for the test stand as it permits operation well below the facility's electrical and thermal capacity constraints. Additionally, the model predicts dry compression with this compressor at the 200 °C process heat delivery condition. An operating speed of 2,000 RPM was selected for use with cyclopentane as the power consumption and refrigerant mass flow rate at this speed align with the modeled system size.

3.2. Heat exchanger selection

Heat exchangers from SWEP are to be used in the test stand. The selected models for each component and geometric characteristics are reported in Table 2.

Table 2. Selected SWEP heat exchangers to be used in the test stand.

Heat Exchanger	Model Number	Number of Plates
Condenser	B120T	210
Evaporator	V80	52
SLHX	B8T	38
Economizer	B5T	16

To ensure proper performance, comparisons between the moving boundary model and the model developed by SWEP were performed. Figure 4 displays the parity plot for the hot and cold side outlet temperatures predicted by each model for each component. The two models demonstrate strong agreement across each component. All predictions fall within the ±5 K bounds, with a mean absolute error of 0.6 K.

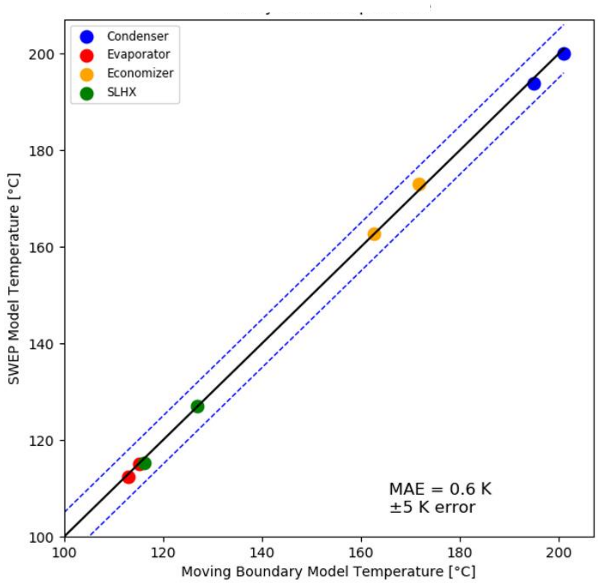

Figure 4. Parity plot for heat exchanger outlet temperatures for the SWEP and moving boundary models.

While this agreement is a strong preliminary validation of the moving boundary modeling approach, experimental data to be gathered from the test stand detailed in Section 3.4 will be required to fully evaluate model accuracy. In general, moving boundary modeling approaches strike a middle ground between fidelity and computational cost, being more detailed than lumped approaches but less detailed than tube-by-tube or segment-by-segment approaches [21]. The moving boundary model captures phase regions missing in lumped approaches, for example, but does not capture the complex heat transfer phenomena associated with changing flow regimes (bubbly, slug, annular, etc.) within two-phase flow.

3.3. Modeling results

Utilizing the compressor map and moving-boundary heat exchanger models enables a high-fidelity characterization of the HERRICK cycle. A summary of relevant performance parameters is displayed in Table 3. Figure 5 shows the predicted logarithmic P–h diagram for cyclopentane under the boundary conditions defined in Table 1. The model confirms that approximately 5 K of superheating and 5 K of subcooling are achievable at heat sink outlet temperatures of 200 °C.

The test stand will be commissioned with R-1336mzz(Z) before testing with cyclopentane to allow a comparison to existing, lower-temperature systems in the literature and on the market. A comparison of performance parameters between the moving boundary heat exchanger model and a simplified fixed temperature difference model was conducted for both R-1336mzz(Z) and cyclopentane. Compressor suction superheat and COP are shown as a function of sink inlet temperature for both refrigerants in Figure 6 and Figure 7, respectively.

Table 3. Modeling Results for the HERRICK cycle.

Parameter	Value	Unit
$\dot{Q}_{condenser}$	40.5	kW
$\dot{W}_{compressor}$	14.2	kW
COP	2.85	-
Second Law Efficiency	48.7	%
Isentropic Efficiency	67.4	%
Volumetric Efficiency	78.1	%
Source Outlet Temperature	113	°C
Sink Outlet Temperature	201	°C

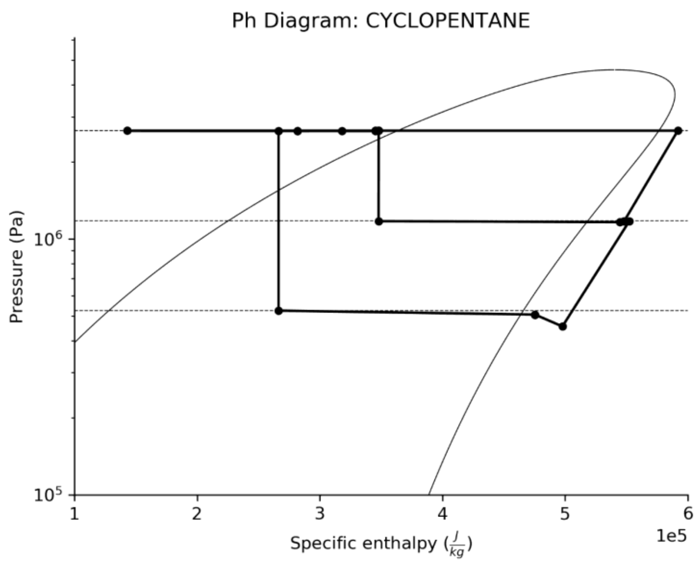

Figure 5. Predicted logarithmic P-h diagram for the HERRICK cycle operating at 200 °C sink temperatures with cyclopentane.

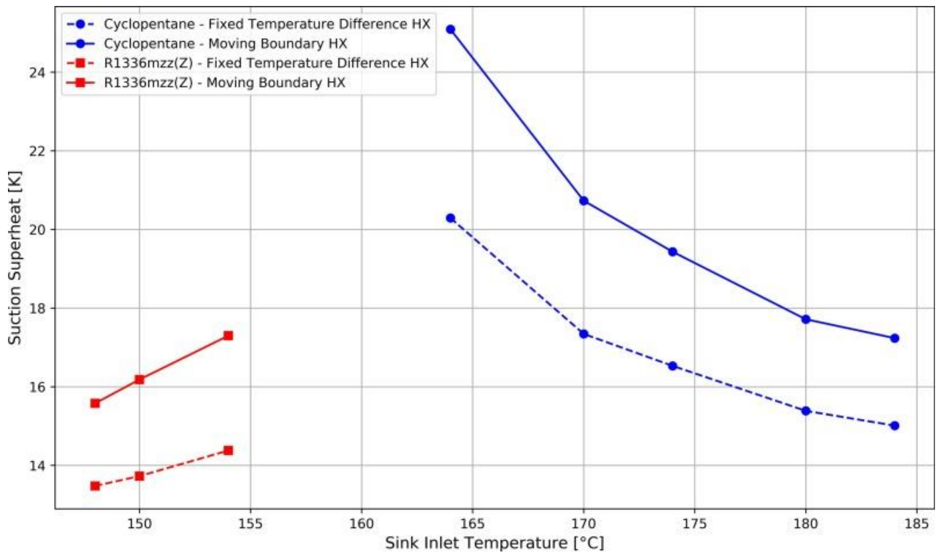

Figure 6. Compressor suction superheat variations between fixed temperature difference and moving boundary heat exchanger models.

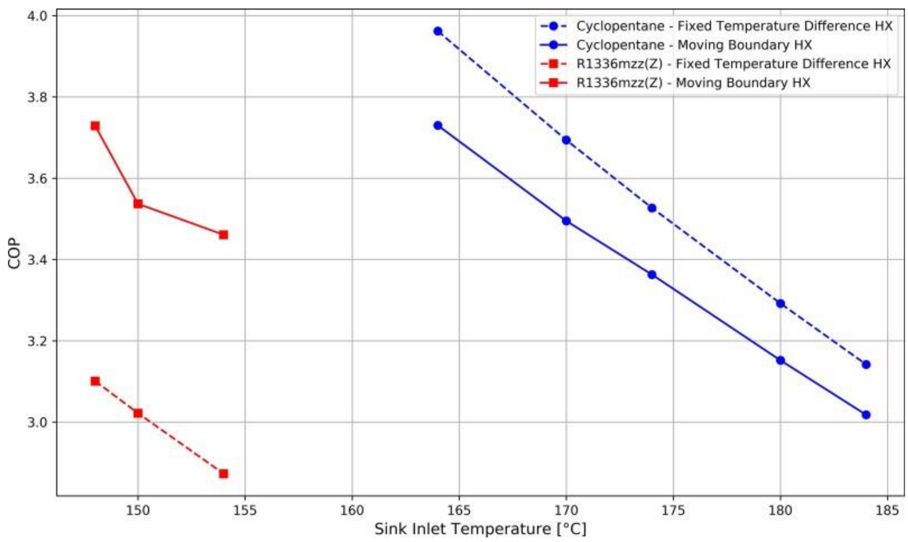

Figure 7. COP variations between the fixed temperature and moving boundary heat exchanger models.

Both models predicted decreasing suction superheat with increasing sink inlet temperature for cyclopentane. The moving boundary model consistently predicted higher suction superheat than the fixed temperature difference model. For cyclopentane, it predicted as much as 5 K higher, and for R-1336mzz(Z), it predicted as much as 2 K higher.

The fixed temperature difference model slightly overpredicted COP for use with cyclopentane due to the lower estimated suction superheat. For R-1336mzz(Z), however, the fixed temperature difference model underpredicted COP by as much as 0.6 (20%). This is because the fixed model underestimated condenser heating capacity and predicted wet compression, leading to a substantial underestimation of system capacity.

3.4. Test stand design

Developing a test stand capable of operating at such extreme temperatures introduces unique design considerations. The heat source, which would be a waste-heat stream in practical deployment, is provided by a circulating water loop heated by the building steam line. Heat rejection occurs through an air-cooled loop of Therminol 66 oil. Regenerative heat transfer is included between the source and sink loops to improve overall system efficiency. Heat will be rejected from the compressor lubricant via a separate cooling loop. The full piping and instrumentation diagram of the test stand is presented in Figure 6.

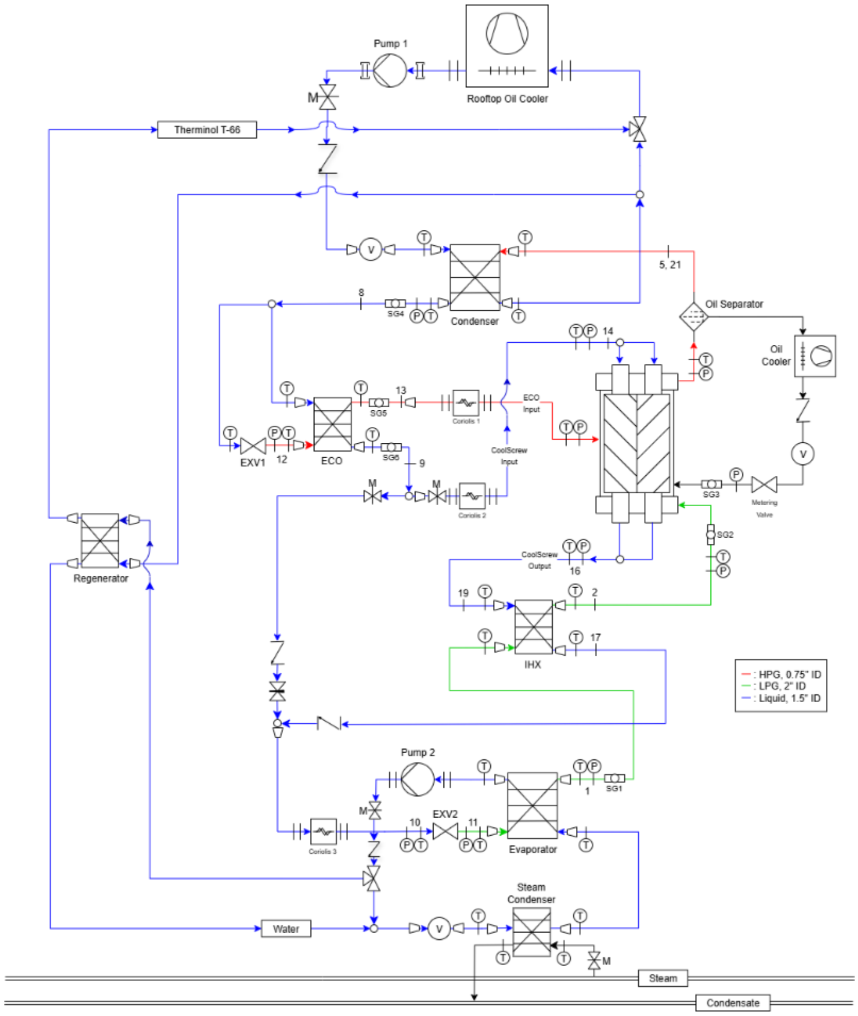

Figure 6. Complete piping and instrumentation diagram for the HERRICK cycle test stand, including heat source and sink loops.

4. Conclusions

This work presented the modeling efforts and test stand design of the novel HERRICK cycle, which utilizes internal refrigerant cooling of the compressor rotors to deliver heat at temperatures up to 200 °C. A refrigerant screening implementing a simplified cycle model revealed cyclopentane to be the working fluid for the test stand. A high-fidelity cycle model implementing discretized moving boundary heat exchanger models and a compressor map was developed to predict key cycle performance parameters. The model predicts a system COP of 2.85, a second law efficiency of 48.7%, and an outlet heat sink temperature of 201 °C. A piping and instrumentation diagram detailing the cycle and its integration into the facility where the test stand is to be built has been prepared. A complete CAD rendering to serve as a reference during the construction phase has also been produced. For future work, the test stand will be brought into operation with the goal of confirming the ability to reach 200 °C heat sink temperatures, informing further development of the high-fidelity model and providing insights into compressor, refrigerant and lubricant interactions.

Acknowledgements

This material is based upon work supported by the U.S. Department of Energy's Office of Energy Efficiency and Renewable Energy (EERE) under the Industrial Technologies Office, Award Number DE-0010864. This work was partially supported by The National Institute of Standards and Technology (NIST), an agency of the United States Department of Commerce.

The authors would like to thank all the project partners for their contributions and support: Penn State University, Chemours, Shrieve, Trane Technologies, Convergent Science.

References

[1] U.S. Energy Information Administration. (n.d.). U.S. energy facts explained. U.S. Department of Energy. https://www.eia.gov/energyexplained/us-energy-facts/

[2] Union, I. (2014). Communication from the Commission to the European Parliament, the Council, the European Economic and Social Committee and the Committee of the Regions. Brussels. http://ww. w. xploit-eu. com/pdfs/Europe, 202020, 20.

[3] International Energy Agency. (2023). *World energy outlook 2023*. OECD Publishing. https://doi.org/10.1787/827374a6-en.

[4] Marina, A., Spoelstra, S., Zondag, H. A., & Wemmers, A. K. (2021). An estimation of the European industrial heat pump market potential. Renewable and Sustainable Energy Reviews, 139, 110545.

[5] Technavio. (2024). Industrial heat pumps market analysis by region (Europe, APAC, North America, Middle East and Africa, South America) and country (US, Italy, China, Japan, Germany, UK, Canada, India, France, Brazil): Size and forecast 2025–2029. https://www.technavio.com/report/industrial-heat-pumps-market-industry-analysis

[6] American Council for an Energy-Efficient Economy. (2023). *Industrial heat pumps*. https://www.aceee.org/industrial-heat-pumps

[7] Arpagaus, C. (2023, July 11). Industrial heat pumps: Technology readiness, economic conditions, and sustainable refrigerants [Conference presentation]. IHP Workshop at the 2023 ACEEE Industrial Summer Study, Eastern Switzerland University of Applied Sciences. https://www.aceee.org/sites/default/files/pdfs/IHP_Workshops_2023/Cordin_Arpagaus_-_OST.pdf

[8] Kondou, C., & Koyama, S. (2015). Thermodynamic assessment of high-temperature heat pumps using Low-GWP HFO refrigerants for heat recovery. International Journal of Refrigeration, 53, 126-141.

[9] Kosmadakis, G., Arpagaus, C., Neofytou, P., & Bertsch, S. (2020). Techno-economic analysis of high-temperature heat pumps with low-global warming potential refrigerants for upgrading waste heat up to 150 C. Energy Conversion and Management, 226, 113488.

[10] Arpagaus, C., Bless, F., & Bertsch, S. S. (2020, July). Theoretical analysis of transcritical HTHP cycles with low GWP HFO refrigerants and hydrocarbons for process heat up to 200 C. In Proceedings of the IIR Rankine Conference, IIR.

[11] Gadagkar, D., Hoess, A. J., Ziviani, D., & Barta, R. B. (2025). Modeling of high-temperature heat pump cycles for industrial applications using moving boundary heat exchangers and advanced cycle architectures. *Applied Thermal Engineering*, 129039.

[12] Spale, J., Hoess, A. J., Bell, I. H., & Ziviani, D. (2024). Exploratory study on low-GWP working fluid mixtures for industrial high temperature heat pump with 200 °C supply temperature. Energy, 308, 132677. https://doi.org/10.1016/j.energy.2024.132677.

[13] Ma, Y., Zhang, B., Hwang, Y. H., Xing, Z., & Radermacher, R. (2011). Research and development of a semi-hermetic reciprocating compressor for transcritical CO_2 refrigeration cycle. Proceedings of the Institution of Mechanical Engineers, Part A: Journal of Power and Energy, 225(1), 101–113. https://doi.org/10.1177/09576509JPE1070

[14] Bell, I. (2011). Plate-heat-exchangers. In ACHP documentation. Retrieved June 3, 2025, from https://achp.readthedocs.io/en/latest/ACHPComponents/PlateHeatExchanger.html

[15] Hou, Weigang; Raeisi Fard, Hafez; Burns, Larry; Groll, Eckhard A.; Ziviani, Davide; and Braun, James E., "Experimental Investigation of R454C as a Replacement for R410A in a Residential Heat Pump Split System" (2022). International Refrigeration and Air Conditioning Conference. Paper 2482. https://docs.lib.purdue.edu/iracc/2482

[16] Martin, H. (2010). N6 Pressure drop and heat transfer in plate heat exchangers. In VDI Heat Atlas (pp. 1515–1522). Springer. https://doi.org/10.1007/978-3-540-77877-6_109.

[17] Cooper, M. G. (1984). Heat flow rates in saturated nucleate pool boiling—a wide-ranging examination using reduced properties. Advances in Heat Transfer, 16, 157–239. https://doi.org/10.1016/S0065-2717(08)70205-3

[18] Claesson, J., 2004. Thermal and Hydraulic Performance of Compact Brazed Plate Heat Exchangers Operating as Evaporators in Domestic Heat Pumps. PhD Thesis. KTH.

[19] Lockhart, R. W., & Martinelli, R. C. (1949). Proposed correlation of data for isothermal two-phase, two-component flow in pipes. Chemical Engineering Progress, 45, 39–48.

[20] Longo, G. A. (2009). Heat transfer and pressure drop during HFC refrigerant saturated vapour condensation inside a brazed plate heat exchanger. International Journal of Heat and Mass Transfer, 52(1–2), 402–411. https://doi.org/10.1016/j.ijheatmasstransfer.2009.11.003.

[21] Sarfraz, Omer; Bach, Christian K.; and Bradshaw, Craig, "A Literature Review of Numerical Modeling Techniques for Vapor Compression Systems with Focus on Heat Exchanger Modeling" (2018). International Refrigeration and Air Conditioning Conference. Paper 1966. https://docs.lib.purdue.edu/iracc/1966